International Journal of Thermofluid Science and Technology (2022)
Volume 9, Issue 4, Paper No. 090402
https://doi.org/10.36963/IJTST.2022090402
Research Article

On the behavior of the flow field components from the momentum equation for a functioning model of rocket motors

Gabriel Kaldjob Pom[1], Jacques Hona[1,*], Valjacques Nyemb Nsoga[1], Médard Marcus Nganbe II[1]

[1]*Applied Mechanics Laboratory, Faculty of Science, University of Yaoundé I, P.O. Box 812, Yaoundé, Cameroon*

ATICLE INFO

Received: 24 Dec. 2021;
Received in revised form:
07 Jul. 2022;
Accepted: 10 Jul. 2022;
Published online:
20 July 2022

Keywords:
Rocket motor model
Suction-driven flow
Navier-Stokes equations
Nonlinear ordinary differential equations
Numerical solutions

ABSTRACT

In this study, a fluid is expelled by the suction process from the intermediate space between to porous plates in transverse movement in order to model the functioning of a compartment of a rocket motor. This transverse motion of the plates can reduce or increase the flow domain in order to enhance the performance of the motor. From a theoretical point of view which is the present contribution, the problem is described by the velocity and the pressure gradient known as the flow field components which are determined under different values of the Reynolds number and the expansion or contraction ratio representing the control parameters of the problem. It is found that, the decrease of the magnitude of the axial pressure gradient by expanding the space occupied by the fluid causes flow reversal in the case of low suction Reynolds numbers. The reduction of the flow domain increases the magnitude of the axial pressure gradient and destroys the backward flow for all the suction Reynolds numbers. This reduction or contraction of the flow field causes a linear profile of the radial velocity and a linear behavior of the axial pressure gradient.

1. Introduction

The movement of liquids and gases is widely studied because fluid flows are on the basis of the functioning of many natural, biological and industrial systems [1-9]. In particular, the flows in the vicinity of the permeable walls are used to model filtration, solar energy collectors, boundary layer separation, slab rocket motors, as well as biological transport processes. In this context of the flows occurring near permeable walls, the dynamics of the fluid is influenced by the porosity of the flow boundaries. This influence is perceptible through the boundary conditions of the problem. The porous walls delimiting the flow can also be mobile. At this stage, it is convenient to consider a global theme that consists of three types of fluid flows, notably the flows in the vicinity of fixed permeable walls [10-12], and the flows in the neighborhood of impermeable moving walls

[*]*Corresponding e-mail*: honajacques@yahoo.fr (Jacques Hona)

Nomenclature

a	half-width of the flow domain, m	r_ρ	solid-to-fluid density ratio
a_0	initial half-width of the flow domain, m	u_m	mean flow velocity through the lateral cross-section, m/s
V	absolute fluid speed at walls, m/s	r^*	nondimensional radial coordinate
V_s	relative suction velocity, m/s	u^*	nondimensional radial veocity
$\dot{a}$	displacement velocity of the walls, m/s	w^*	nondimensional normal velocity
$\dot{a}_0$	initial expansion/contraction rate, m/s	p^*	nondimensional pressure
r	radial coordinate, m	F	nondimensional stream function
z	normal coordinate, m	*Greek symbols*	
t	time, s	η	nondimensional normal variable
u	radial velocity, m/s	ϑ	volume of the flow domain, m^3
w	normal velocity, m/s	ρ	specific mass of the fluid, kg/m^3
p	pressure, Pa	ρ_0	propellant specific mass, kg/m^3
A_s	sum of suction areas, m^2	ν	kinematic viscosity of the fluid, m^2/s
A_c	lateral surface of the cylindrical flow domain, m^2	ψ	stream function of the problem, m^3/s
E	constant suction coefficient	α	expansion/contraction ratio

[13-15], as well as the flows delimited by both porous and moving walls [7, 16-19]. These three types of flows form the same set of subjects mainly because a seeking solution approach called the similarity method [20] can be relatively used to solve each of the three types of problems taking into account the respective geometrical configurations. Regarding geometrical configurations, it would be interesting to focus the attention on the flows through rectangular and cylindrical conduits which are most encountered in practice. A conduit is said to be rectangular when the cross section of the flow is a rectangle or a square involving the use of a Cartesian coordinate system for the analysis of the movement of the fluid. On the other hand, the flow takes place in a cylindrical domain when it has a longitudinal component and a circular cross-section involving the use of a cylindrical polar coordinate system for the analysis of the dynamics of the fluid.

The similarity method first used by Berman [20] in the study of the flow of a viscous fluid through a rectangular channel having two porous walls has been extended to the investigation of fluid flows in porous cylindrical domains [21-26].

The importance of this method of seeking solutions has led some authors to consider the movements of fluids through rectangular and cylindrical domains with porous boundaries as Berman flows because Berman's pioneering study [20] has inspired many other authors to study planar flows [12, 27-29] and cylindrical flows [21-26, 30], as well as the stability of the flows [31-35]. For the particular case of planar flows, that is the flows which generally admit two velocity components, notably a longitudinal component and a transversal component, Berman assumed that the transversal or normal velocity does not depend on the longitudinal coordinate and that the longitudinal velocity depends both on the longitudinal and transversal coordinates. It appears that, the similarity method of Berman used to investigate the two-dimensional rectangular channel flow [20] was based on a rigorous change of variables relating to the geometry of the flow domain and the boundary conditions. The Berman approach is increasingly used as it validity has been tested experimentally and numerically [34-36]. On the other hand, other approaches to solve the Navier-Stokes equations describing the fluid motions exist [37, 38], notably the finite

difference methods [39, 40] representing a class of numerical techniques for solving differential equations by approximating derivatives with finite differences. Both the spatial domain and time interval are discretized, or broken into a finite number of steps, and the value of the solution at these discrete points is approximated by solving algebraic equations containing finite differences and values from nearby points. More precisely, finite difference methods convert ordinary differential equations (ODE) or partial differential equations (PDE), which may be nonlinear, into a system of linear equations that can be solved by matrix algebra techniques. In the search for solutions of the Navier-Stokes equations for the special case of fluid flows between two porous boundaries, scientists increasingly prefer to use the Berman similarity method [20], because it enables the determination of a large number of flow characteristics, compared to other existing methods [37-40]. These flow characteristics are velocity profiles, the pressure, the pressure gradients, the wall friction coefficient or the wall shear stress coefficient, the stream function, as well as the streamlines [12, 21-24]. In fact, the Navier-Stokes equations [41-44] mathematically express the conservation of momentum and the conservation of mass for Newtonian fluids. They are sometimes accompanied by an equation of state relating pressure, temperature and density; they are also used to investigate complex fluid flows [38] known as the movement of fluids associated with chemical reactions or in the presence of a magnetic field. The difference between the Navier-Stokes equations and the closely related Euler equations is that the Navier-Stokes equations take viscosity into account while the Euler equations model only inviscid flows. The Navier-Stokes equations are useful because they describe the physics of many phenomena of scientific and engineering interests. For example, they may be used to model the weather, ocean currents, water flow in a pipe and air flow around a wing. The Navier-Stokes equations, in their full and simplified forms, help with the design of aircraft and cars, the study of blood flow, the design of power stations, the analysis of pollution, and many other things.

The fluid flows between two walls that are both porous and in motion can be broken down into two sets of problems. The first set of previously studied problems concerns the case where the movement of the fluid takes place in the same direction as the movement of the porous walls [16-18]. The second set of problems constitutes the case where the two porous walls move perpendicular to the movement of the fluid [7, 19]. In the two sets of problems, the moving porous walls that represent the boundaries of the fluid flow may be the rectangular surfaces or the lateral surfaces of the cylinders. It is in this context of the fluid flows between two moving porous walls that the present work is situated, with the novelty that the two moving porous boundaries are the circular permeable plates instead of the rectangular surfaces or the lateral surfaces of cylinders which characterize previous works.

The two circular plates translate along the same axis passing perpendicular to the midpoints of their respective surfaces when the flow takes place in their intermediate space with a suction phenomenon at their porous walls. Indeed, the suction phenomenon is the removal of mass of fluid from the porous geometric domain containing the moving fluid. The phenomenon contrary to suction is the injection [45] which characterizes the mass addition of fluid in the flow field. The flow studied in the present work incorporates the phenomenon of suction by assuming that the mass of fluid exiting the flow domain is equal to that entering it. In this case, the flow is described by applying the conservation of mass and the conservation of momentum. The conservation of mass leads to the continuity equation, while the conservation of momentum gives rise to the Navier-Stokes equations. Moreover, the translational movement of the porous circular plates that we consider in this work has the geometric consequence of reducing or increasing the volume of the flow domain. More precisely, the translational movement of the discs can move them away or closer together causing respectively an increase or a reduction in volume of the flow domain. At this stage, it is convenient to note

that the purpose of this study is the determination of the influences of the porosity of the flow boundaries and the increase or decrease in volume of the flow domain on the characteristics of the fluid movement. The attention is focused on the characteristics that intervene directly in the equations governing the problem, notably the velocity components and the pressure gradient which describe the continuity equation and the Navier-Stokes equations. The determination of these characteristics of the flow results from an organization of this work which considers the present introduction as Section 1. The presentation of the governing equations associated with the description of the geometry of the flow is the subject of Section 2. Section 3 is devoted to the similarity transformation of the governing equations and the introduction of nondimensional variables. The numerical results are presented and discussed in Section 4. The conclusion intervenes in Section 5.

2. Mathematical description

The problem is similar to a two-dimensional flow described by a velocity component parallel to the walls of the circular surfaces called the radial velocity *u*, and another velocity component perpendicular to the surfaces of the discs known as the axial or normal velocity *w*, as well as the pressure field *p* related to the two velocity components due to the momentum conservation. Due to the described geometry of the movement of the fluid, it appears that the flow is axisymmetric and the coordinate system (*r*, *z*) is derived to model the dynamics of the fluid between two circular plates or discs situated at $z = -a(t)$ and $z = +a(t)$ as shown in Fig. 1. Hence, $2a(t)$ is the distance between the plates and $a(t)$ denotes the half-width of the flow domain depending on the time *t*. As the fluid moves in the space between the two porous plates, a mass of fluid is expelled through the pores of these plates at the absolute speed *V* that depends on the relative suction velocity V_s and the displacement velocity of the porous walls $\dot{a}$

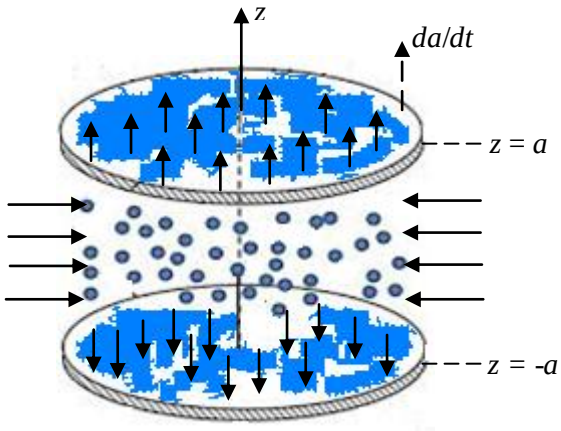

Fig. 1. Sketch of the flow domain

defined by $\dot{a} = da/dt$, such that:

$$V = V_s - \dot{a} \tag{1}$$

The displacement velocity $\dot{a}$ of the porous walls also known as the entrainment velocity of fluid particles near the permeable surfaces is positive in the expansion case and negative for contraction.

By neglecting gravity terms [21-26] due to the fact that the fluid layer between the circular surfaces and the width of the flow domain are small compared to the same radius of the discs which tends to infinity, the equations of motion are given by:

$$\frac{1}{r}\frac{\partial}{\partial r}(ru) + \frac{\partial w}{\partial z} = 0 \tag{2}$$

$$\frac{\partial u}{\partial t} + u\frac{\partial u}{\partial r} + w\frac{\partial u}{\partial z} = -\frac{1}{\rho}\frac{\partial p}{\partial r} + \nu\left(\frac{1}{r}\frac{\partial}{\partial r}\left(r\frac{\partial u}{\partial r}\right) + \frac{\partial^2 u}{\partial z^2} - \frac{u}{r^2}\right) \tag{3}$$

$$\frac{\partial w}{\partial t} + u\frac{\partial w}{\partial r} + w\frac{\partial w}{\partial z} = -\frac{1}{\rho}\frac{\partial p}{\partial z} + \nu\left(\frac{1}{r}\frac{\partial}{\partial r}\left(r\frac{\partial w}{\partial r}\right) + \frac{\partial^2 w}{\partial z^2}\right) \tag{4}$$

where ρ and ν denote respectively the specific mass and the kinematic viscosity known as the physical properties of the working fluid. The

problem is stated such that, the radial motion of fluid particles vanishes in the close vicinity of the porous walls, that is the no slip condition. In addition, the fluid is equally distributed on the both sides of the circular midsection of the flow domain known as the open wall situated at $z = 0$, that is the sandwiched flow. Finally, as the problem pertains to a sandwiched flow, equal suction fluxes of fluid need to be considered at both porous walls. This description gives rise to the following boundary conditions:

$$\begin{array}{llll} u = 0, & w = +V & \text{for} & z = a(t) \\ \dfrac{\partial u}{\partial z} = 0, & w = 0, & \text{for} & z = 0 \\ u = 0, & w = -V & \text{for} & z = -a(t) \end{array} \quad (5)$$

The two discs are uniformly porous such that A_s is the sum of the suction areas defined by: $A_s = \pi r^2 + \pi r^2 = 2\pi r^2$. By referring to the application of the active propellants with ρ_0 as the propellant specific mass, the conservation of mass at the burning surface A_s, expressed as $\rho A_s V_s = \rho_0 A_s \dot{a}$ [7, 46], gives birth to the solid-to-fluid density ratio $r_\rho = \dfrac{\rho_0}{\rho}$ related to the relative suction velocity V_s at walls by the following expression: $V_s = \left(\dfrac{\rho_0}{\rho}\right)\dot{a} = r_\rho \dot{a}$. Considering Eq. (1), the absolute fluid withdrawal speed V and the fluid particle entrainment velocity at walls $\dot{a}$ are related as follows: $V = (r_\rho - 1)\dot{a} = E\dot{a}$, where $E = r_\rho - 1$ is the constant suction coefficient estimated for example in rocket motors to be $E = 99$ for a typical $\rho_0 = 2000\ \text{kgm}^{-3}$ and $\rho = 20\ \text{kgm}^{-3}$ [7, 46-48]. On the other hand, the volume of the flow domain which is a cylinder of radius r and of length $2a$ is defined as: $\vartheta = \pi r^2 2a = \dfrac{1}{2}A_c r$, where A_c is the lateral surface of the cylindrical flow domain given by: $A_c = 2\pi r(2a) = 4\pi r a$. At this stage, it is important to note that the mass of fluid which enters the flow domain with the mean velocity u_m through the lateral cross section A_c is expressed in terms of the remaining mass and the mass exiting the flow field through the suction area A_s, this leads to the flow rate equation:

$$\rho u_m A_c = \frac{\partial}{\partial t}\int_\vartheta \rho d\vartheta - \rho V_s A_s \quad (6)$$

By taking into account the expression of the volume of the flow field $\vartheta = \dfrac{1}{2}A_c r$, Eq. (6) becomes:

$$\rho u_m A_c = \frac{\partial}{\partial t}\left(\frac{1}{2}\rho A_c r\right) - \rho V_s A_s \quad (7)$$

As the flow rate equation is established at a given radius r, this leads to the following equation:

$$\rho u_m A_c = \frac{1}{2}\rho r\frac{\partial A_c}{\partial t} - \rho V_s A_s \quad (8)$$

It is relevant at this stage to define the mean flow velocity u_m as follows:

$$u_m = \frac{1}{2}\frac{r}{A_c}\frac{\partial A_c}{\partial t} - \frac{A_s}{A_c}V_s \quad (9)$$

Considering the expressions of the surfaces $A_c = 4\pi r a$ and $A_s = 2\pi r^2$, another expression of the mean velocity is:

$$u_m = \frac{1}{2}\frac{r}{a}\dot{a} - \frac{1}{2}\frac{r}{a}V_s = \frac{1}{2}\frac{r}{a}(\dot{a} - V_s) \quad (10)$$

In light of Eq. (1), a simplified expression of u_m is:

$$u_m = -\frac{1}{2}\frac{r}{a}V \quad (11)$$

Equation (11) shows that the mean flow velocity u_m depends on the radius of the discs, the width of the flow domain and the absolute suction speed at porous walls.

The fact that the flow field of the incompressible fluid presents two velocity

components involves the existence of the stream function ψ defined as:

$$u = \frac{1}{r}\frac{\partial \psi}{\partial z}, \qquad w = -\frac{1}{r}\frac{\partial \psi}{\partial r} \tag{12}$$

It is important to note and easy to verify that, as the stream function exists, the continuity Eq. (2) is self satisfied. On the other hand, the two Navier-Stokes Eqs. (3) and (4) are transformed into a single equation of vorticity describing the same problem as:

$$\frac{\partial}{\partial t}\left(D^2\psi\right)+\frac{1}{r}\left(\frac{\partial \psi}{\partial z}\frac{\partial}{\partial r}\left(D^2\psi\right)-\frac{\partial \psi}{\partial r}\frac{\partial}{\partial z}\left(D^2\psi\right)\right) - \frac{2}{r^2}\frac{\partial \psi}{\partial z}D^2\psi = \nu D^4\psi \tag{13}$$

where $D^2\psi = \frac{\partial^2 \psi}{\partial z^2} + r\frac{\partial}{\partial r}\left(\frac{1}{r}\frac{\partial \psi}{\partial r}\right)$. The boundary conditions related to Eq. (13) are derived:

$$\begin{aligned} &\frac{1}{r}\frac{\partial \psi}{\partial z} = 0, \quad -\frac{1}{r}\frac{\partial \psi}{\partial r} = +V \quad \text{for } z = a(t) \\ &\frac{1}{r}\frac{\partial^2 \psi}{\partial z^2} = 0, \quad -\frac{1}{r}\frac{\partial \psi}{\partial r} = 0 \quad \text{for } z = 0 \\ &\frac{1}{r}\frac{\partial \psi}{\partial z} = 0, \quad -\frac{1}{r}\frac{\partial \psi}{\partial r} = -V \quad \text{for } z = -a(t) \end{aligned} \tag{14}$$

3. Transformation of the vorticity equation

This stage is devoted to the transformation of the partial differential Eq. (13) into an ordinary differential equation for the same problem by means of a similarity method as follows:

$$\psi(r,z,t) = \frac{1}{2}\frac{\nu}{a}r^2F(\eta,t), \quad \eta = \frac{z}{a(t)} \tag{15}$$

where F is a similarity solution in space, η denotes the nondimensonal axial variable. Thus, in terms of function F, the vorticity Eq. (13) and boundary condition (14) become:

$$\frac{\partial^4 F}{\partial \eta^4} - \frac{\partial F}{\partial \eta}\frac{\partial^2 F}{\partial \eta^2} + F\frac{\partial^3 F}{\partial \eta^3} + 3\alpha\frac{\partial^2 F}{\partial \eta^2} + \alpha\eta\frac{\partial^3 F}{\partial \eta^3} - \frac{a^2}{\nu}\frac{\partial}{\partial t}\left(\frac{\partial^2 F}{\partial \eta^2}\right) = 0 \tag{16}$$

$$\begin{aligned} &\frac{\partial F}{\partial \eta}(+1,t) = 0, \; F(+1,t) = -\frac{a(t)V}{\nu} \quad \text{for } \eta = +1 \\ &\frac{\partial^2 F}{\partial \eta^2}(0,t) = 0, \; F(0,t) = 0 \quad \text{for } \eta = 0 \\ &\frac{\partial F}{\partial \eta}(-1,t) = 0, \; F(-1,t) = +\frac{a(t)V}{\nu} \quad \text{for } \eta = -1 \end{aligned} \tag{17}$$

where a nondimensional parameter $\alpha = \frac{a\dot{a}}{\nu}$ deriving from the displacement of the flow boundaries called the expansion or the contraction ratio is introduced. The parameter α is positive in the expansion case and negative for the contraction. The boundary conditions (17) are established whatever the time t. Equation (16) subject to boundary conditions (17) needs an initial condition to be solved, but this initial condition does not interest the dynamics discussed in the current work, because the similarity problem in space presented in Eqs. (16) and (17) is only a step of passage to obtain a problem described by an ordinary differential equation by assuming that the function F is made dependent on η instead of (η,t) in order to obtain a similarity solution in space and time, this implies the expression $\frac{\partial}{\partial t}\left(\frac{\partial^2 F}{\partial \eta^2}\right) = 0$, by setting α to be constant or quasi-constant in time. In that event, the value of the expansion or contraction ratio α can be specified by its initial value $\alpha = \frac{a\dot{a}}{\nu} = \frac{a_0\dot{a}_0}{\nu}$, where a_0 and $\dot{a}_0$ denote the initial half-width of the flow domain and expansion/contraction rate, respectively. If $\alpha = \frac{a\dot{a}}{\nu} = \frac{a_0\dot{a}_0}{\nu}$ is assumed to be constant, by taking into account the relation $V = E\dot{a}$, the expression of the Reynolds number for the similarity solution in space and time is $R = \frac{aV}{\nu} = E\alpha$, considering a

constant value of the suction coefficient *E*. In the present study, the constant value of *E* is not given, because this work does not concern a particular fluid, but it is a general contribution to a better understanding of incompressible fluid flows between two expanding or contracting porous walls in the model of rocket motors. In fact, two types of motions are combined in the current study, notably the movement of the discs and the movement of the fluid. Hence, the parameter α can be considered as a sort of Reynolds number related to the displacement of the circular porous plates. As *F*, α and *R* do not explicitly depend on time *t*, the problem to solve becomes:

$$F^{(4)} - F^{(1)}F^{(2)} + FF^{(3)} + 3\alpha F^{(2)} + \alpha\eta F^{(3)} = 0 \tag{18}$$

$$F^{(1)}(+1) = 0\,,\ F(+1) = -\frac{aV}{\nu} = -R \ \text{ for } \eta = +1$$

$$F^{(2)}(0) = 0\,,\ F(0) = 0 \quad \text{for} \quad \eta = 0 \tag{19}$$

$$F^{(1)}(-1) = 0\,,\ F(-1) = +\frac{aV}{\nu} = +R \ \text{ for } \eta = -1$$

where $F^{(i)} = d^i F / d\eta^i$. In terms of function *F*, the two velocity components are derived:

$$u = \frac{1}{2}\frac{\nu\, r}{a^2}F^{(1)}(\eta)\,, \quad w = -\frac{\nu}{a}F(\eta) \tag{20}$$

In the current flow configuration, the radial velocity is made dimensionless by means of the mean flow velocity u_m and the axial velocity is determined in unit of the absolute suction speed *V*, such that:

$$u^* = \frac{u}{u_m} = -F^{(1)}(\eta)/R\,,\ w^* = \frac{w}{V} = -F(\eta)/R \tag{21}$$

In this work, obtaining the vorticity equation satisfied by the stream function involves the disappearance of pressure terms of the momentum equation. However, since the stream function is related to the velocity components by assuming the incompressibility of the working fluid, the similarity expression corresponding to the radial pressure gradient per unit radius can be derived by substituting Eqs. (20) into Eq. (3) as follows:

$$\frac{1}{r}\frac{\partial p}{\partial r} = \frac{1}{2}\rho\frac{\nu^2}{a^4}\left(F^{(3)} + FF^{(2)} + \left(2\alpha - F^{(1)}\right)F^{(1)} + \alpha\eta F^{(2)}\right) \tag{22}$$

The half-width of the flow domain *a* is used to normalized the lengths, such that: $r^* = r/a$ and $z^* = \eta = z/a$. In addition, the pressure is made dimensionless by the reference pressure (ρV^2) as $p^* = p/(\rho V^2)$. This leads to define the nondimensional radial pressure gradient per unit radius by the formulas:

$$\frac{1}{r^*}\frac{\partial p^*}{\partial r^*} = \frac{1}{2}\left(F^{(3)} + FF^{(2)} + \left(2\alpha - F^{(1)}\right)F^{(1)} + \alpha\eta F^{(2)}\right)/R^2 = \text{cte} \tag{23}$$

Equation (23) reveals that the nondimensional radial pressure gradient per unit radius is constant inside the flow field as it is equivalent to the integral form of Eq. (18) at a given Reynolds number. On the other hand, the expression of the axial pressure gradient in terms of function *F* and its derivatives is obtained by introducing the formulas (20) in Eq. (4) as follows:

$$\frac{\partial p}{\partial z} = -\frac{\rho\nu^2}{a^3}\left(\alpha F + \alpha\eta F^{(1)} + F^{(2)} + FF^{(1)}\right) \tag{24}$$

Considering the references of lengths *a* and pressure (ρV^2), such that $\eta = z/a$ and $p^* = p/(\rho V^2)$ the nondimension axial pressure gradient is given by:

$$\frac{\partial p^*}{\partial \eta} = p^{(1)*}(\eta) = -\left(\alpha F + \alpha\eta F^{(1)} + F^{(2)} + FF^{(1)}\right)/R^2 \tag{25}$$

In this work, as the function *F* derives from the stream function by similarity transformation, the incompressibility of the fluid that relates the function ψ and the

velocity components involves also the relationships of the function F with the radial and normal velocities. On the other hand, the expressions of u and w in terms of F involves the definitions of the radial pressure gradient per unit radius and the normal or axial pressure gradient in terms of the function F and its derivatives by using the Navier-Stokes equations.

4. Results from the numerical integration and discussion

The numerical solution is obtained by integration of Eq. (18) and boundary conditions (19) using the shooting method associated with the fourth-order Runge-Kutta scheme [49]. As the sandwiched flow develops in a symmetric domain, Eq. (18) is solved in the interval [0, 1] considering the boundary conditions:

$$F^{(1)}(+1) = 0\,,\ F(+1) = -R \quad \text{for} \quad \eta = +1$$
$$F^{(2)}(0) = 0\,, \qquad F(0) = 0 \quad \text{for} \quad \eta = 0 \quad (26)$$

The global solution in the entire flow domain [-1, 1] is derived by symmetry. In this paper, the numerical results pertain to the flow characteristics which directly influence the momentum conservation, notably the profiles of the radial velocity and the axial or normal velocity, as well as the normal pressure gradient. These flow characteristics derive from the Navier-Stokes equations that express a relationship between inertia, viscous and pressure terms in the absence of gravity forces as the width of the flow domain is small.

4.1 Radial velocity profile

The radial velocity is presented in Figs. 2–4 for different values of the control parameters of the problem. Indeed, for a fixed low Reynolds number as shown in Fig. 2, flow reversal also known as the backward flow manifests inside the flow domain for large expansion ratio. At this stage, it is convenient to note that the expansion is considered to be large with respect to the value of the Reynolds number. This means that the primary direction of motion of the flow changes as the expansion ratio is relatively important compared to the Reynolds number as shown in Fig. 2.

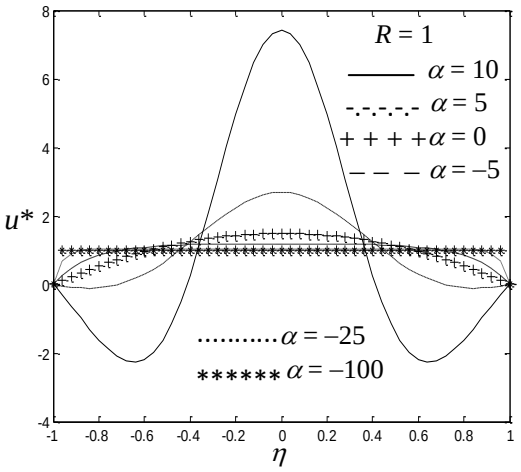

Fig. 2. Radial velocity component for a fixed low Reynolds number R = 1, under different values of the expansion or contraction ratio.

More precisely, the expansion corresponds to positive values of the nondimensional parameter α, while the contraction pertains to negative values of this parameter. It follows that Fig. 2 is performed under different values of the expansion and contraction ratios at a fixed low Reynolds number.

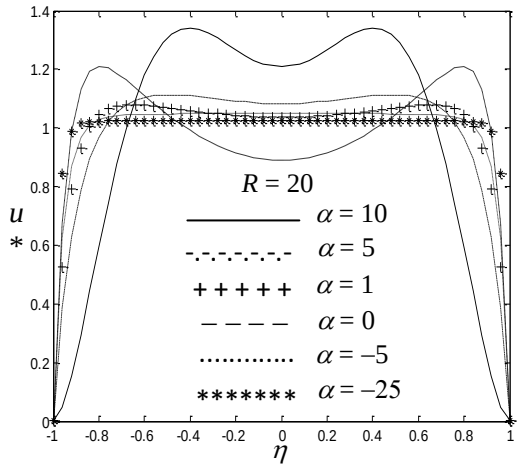

Fig. 3. Radial velocity component for a fixed Reynolds number R = 20, under different values of the expansion or contraction ratio.

Large expansion which results from the increase in volume of the flow domain causes

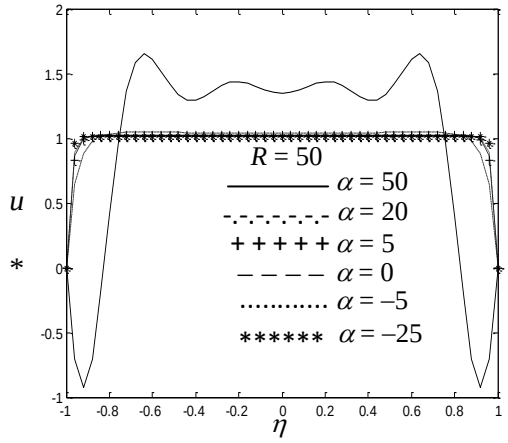

Fig. 4. Radial velocity component for a fixed Reynolds number R = 50, under different values of the expansion or contraction ratio.

flow reversal which manifests itself as negative values of the radial velocity u^* near the porous walls.

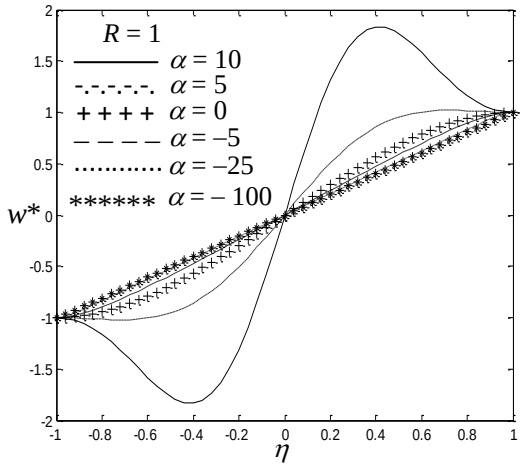

Fig. 5. Axial or normal velocity component for a fixed low Reynolds number R = 1, under different values of the expansion or contraction ratio.

For the same values of the control parameters involving the manifestation of the backward flow in the neighborhood of the discs, the magnitude of the radial velocity is maximal around the middle of the flow domain. In fact, the flow reverses in an attempt to occupy the empty space created by the increase in volume of the flow field as the suction Reynolds is relatively small compared to the expansion ratio. Another understanding of the phenomenon of the backward flow is that, the rapid expansion of the flow boundaries slows the movement of fluid particles near the porous walls, but accelerates the motion of fluid particles close to the middle of the flow field. The empty space caused by the expansion of the flow field is created near the porous walls, since the fluid turns back to fill the vacuum that only occurs close to the boundaries. Indeed, this is understandable, because as it is the movement of the walls which causes the vacuum, it is geometrically convincing that this vacuum is first perceptible in the vicinity of the walls, reason why in Fig. 2 the radial velocity increases with the parameter α near the middle of the flow field while a decrease is observed in the neighborhood of the walls.

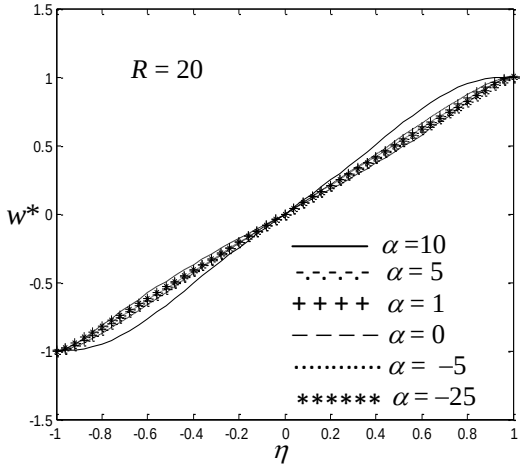

Fig. 6. Axial or normal velocity component for a fixed Reynolds number R = 20, under different values of the expansion or contraction ratio.

When the expansion ratio is not relatively important compared to the Reynolds number, the regions of negative values of the radial velocity disappear inside the flow field due to the absence of flow reversal as shown in Fig. 3. It is convenient to note that although the value R = 20 is moderate, the backward flow ceases to manifest within the flow domain, because in this case the suction motion is important compared to the displacement of the discs

corresponding to the increase in volume of the space containing the moving fluid.

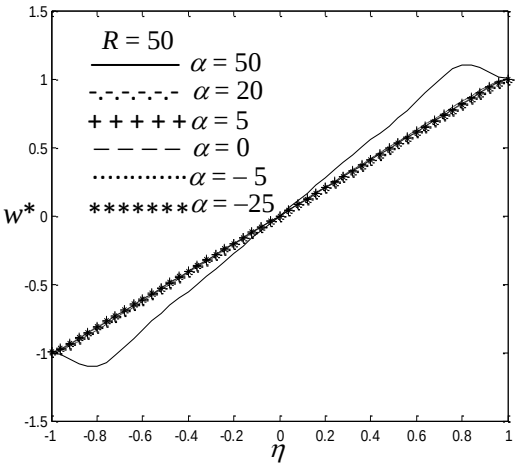

Fig. 7. Axial or normal velocity component for a fixed Reynolds number R = 50, under different values of the expansion or contraction ratio.

The comparison of Fig. 2 with Fig. 3 reveals that, although flow reversal occurs in the flow field, the expansion process dominates the suction phenomenon as presented in Fig. 2, the magnitude of the radial velocity increases in the central region of the space containing the fluid, but this magnitude decreases in Fig. 3 due to the growth of the Reynolds number involving the disappearance of the backward flow as the influence of the augmentation in volume of the flow domain on the fluid motion is reduced compared to the suction phenomenon. For added clarity, the results from the numerical integration show that, in this work, flow reversal or the backward flow seems to occur within the flow domain as the relative suction ratio α/R is great or equal to 1, such that $\alpha/R \geq 1$. In light of Figs. 2–4, the increase in the suction Reynolds by expanding the space containing the fluid tends to create an oscillatory behavior of the radial velocity component, on one hand. On the other hand, for all the values of the Reynolds number, the contraction involves the flattening of the radial velocity profiles.

4.2 Normal velocity profile

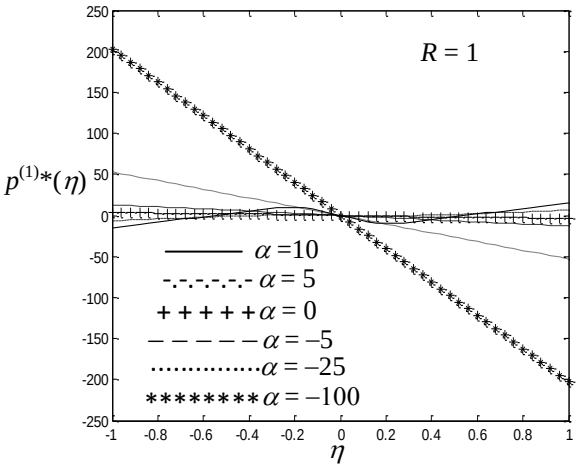

Fig. 8. Axial or normal pressure gradient for a fixed low Reynolds number R = 1, under different values of the expansion or contraction ratio.

The curves corresponding to the normal or axial velocity profiles are presented in Figs. 5–7 under different values of R and α. As the expansion is important compared to suction, such that $\alpha/R \geq 1$, Fig. 5 shows some regions inside the flow domain where the magnitude of the normal velocity w^* exceeds its value at walls due to the same values of the control parameters R and α involving the backward flow. As the expansion of the flow boundaries takes place in the direction transverse to the surfaces of the discs, the fact that the normal velocity which is also the transverse velocity overflows its established value through the boundary conditions reveals that the fluid particles are all the more transversely driven as the suction is weak. In this case the flow is similar to the entrainment movement of the fluid particles caused by the transverse displacement of the porous walls. It appears in other words that the influence of the increase in volume of the flow domain on the movement of the fluid is more noticeable for a weak suction. However, the increase in the Reynolds number involving the disappearance of the weak suction reduces the influence of the expansion of the walls on the fluid flow. Thus, it appears that the phenomena of suction and expansion of the walls are antagonistic in the problem under study. On the other hand, for small, moderate and high Reynolds

numbers, the contraction in volume of the flow field causes a linear profile of the normal velocity as shown in Figs. 5–7. For more details, the results from the numerical integration enable to observe that, as the suction Reynolds number is successively increased above 20, the normal velocity becomes increasingly more linear by approaching its expected behavior for an inviscid suction flow $w^* = \eta$ [6, 51]. For this reason, large suction cases are not always shown whenever the corresponding curves are found to cluster very near the inviscid solution.

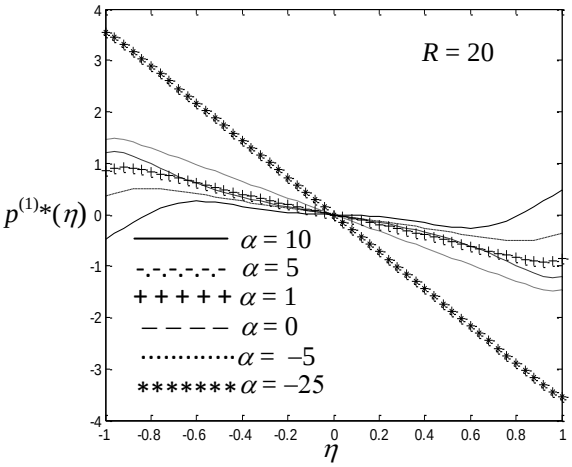

Fig. 9. Axial or normal pressure gradient for a fixed Reynolds number R = 20, under different values of the expansion or contraction ratio.

4.3 Pressure gradients

This stage is devoted to show that the behaviors of pressure gradients presented in Figs. 8–10 are related to those of velocity components due to the momentum conservation giving rise to the Navier-Stokes equations. Indeed, the flow reverses for a low suction because of a weak pressure gradient caused by the expansion in volume of the space containing the fluid according to Fig. 8. More precisely, it is well known that as the distance between the two discs increases due to the expansion process, the pressure gradient diminishes. Thus, the diminution of the pressure gradient slows the movement of the fluid by involving the backward flow in some regions within the flow domain. The described behavior is illustrated in Fig. 8 where the pressure gradient plotted for a low fixed Reynolds number R = 1 takes small values under different values of the expansion ratio α. These values of the normal pressure gradient cease to be small for high contraction due to the reduction in volume of the flow field that destroys flow reversal. It follows that the reduction in volume of the flow domain augments the normal pressure gradient. This augmentation of the normal pressure gradient which manifests itself as great variations tends to increase the movement of the fluid being limited to a flat profile of the radial velocity. It appears from Figs. 8–10 that the normal pressure gradient presents a linear behavior as the volume of the space containing the fluid is reduced. By increasing the Reynolds number, Fig. 10 shows that the normal pressure gradient decreases in the flow domain although it presents great variations for high contraction, while an increase is observed for high expansion.

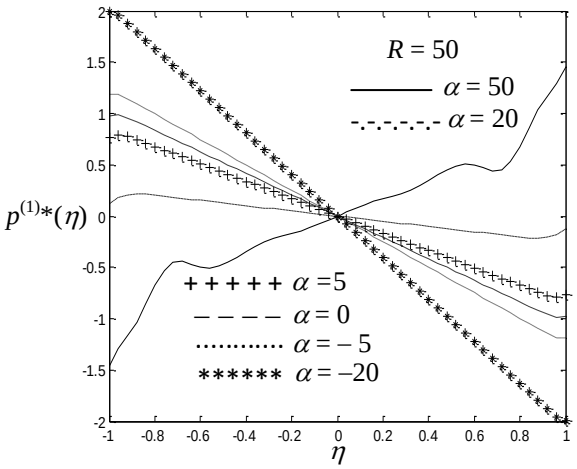

Fig. 10. Axial or normal pressure gradient for a fixed Reynolds number R = 50, under different values of the expansion or contraction ratio.

5. Conclusion

In order to study the suction-driven flow between two identical porous discs that move along the same axis passing at the midpoints of their respective surfaces, the Navier-Stokes equations are used. Since the flow is

axisymmetric and the working fluid is incompressible, the stream function is prescribed in the governing equations in order to transform the problem described by the velocity components and pressure into a single equation satisfied by this stream function. As the vorticity equation satisfied by the stream function is a Partial Differential Equation (PDE), a method of similarity solution taking into account the geometry of the flow domain, the boundary conditions and the physical properties of the fluid is applied to transform the vorticity equation into an Ordinary Differential Equation (ODE) describing the same problem. Thus, the investigation of the dynamics of the fluid is restricted to solving a two-point boundary value problem. To achieve solutions, a numerical scheme based on the rapidly converging shooting method associated with a fourth-order Runge-Kutta algorithm is applied. These solutions are represented in terms of the radial and normal velocity components, as well as the normal pressure gradient. The results obtained show that a high expansion of the flow domain in the case of a low fixed Reynolds number causes flow reversal characterized by the presence of some regions of negatives values of the radial velocity. However, the increase in the suction Reynolds number prevents the manifestation of the backward flow as long as the relative suction ratio α / R is less than 1. The contraction of the volume of the space containing the fluid causes a flattening of the curves corresponding to the radial velocity, while the normal velocity tends to satisfy a linear law.

Due to a high expansion ratio in the case of a low fixed Reynolds number, the variations of the normal pressure gradient are reduced. On the other hand, these variations of the normal pressure gradient become more significant by contracting or expanding the volume of the space containing the fluid in the case of high values of the suction Reynolds number, with the difference that the normal pressure gradient decreases for a high contraction and increases for a high expansion.

References

[1] M.J. Lighthill, Physiological fluid dynamics: a survey, Journal of Fluid Mechanics A 52(3) (1972) 475-497.

[2] M.J. Noroozi, A. Emamifar, A new nonlinear solution for non-Fourier heat transfer in porous fins, International Journal of Thermofluid Science and Technology 8(4) (2021) 080405.

[3] Z. Jalilvand, F.Z. Ashtiani, A. Fouladitajar, H. Rezaei, Computational fluid dynamics modeling and experimental study of continuous and pulsatile flow in flat sheet microfiltration membranes, Journal of Membrane Science 450 (2014) 207-214.

[4] N. Manjunatha, R. Sumithra, R.K. Vanishree, Combined effects of nonuniform temperature gradients and heat source on double diffusive Benard-Marangoni convection in a porous-fluid system in the presence of vertical magnetic field, International Journal of Thermofluid Science and Technology 8(1) (2021) 080104.

[5] M. Abdelkader, H. Ameur, Y. Menni, Investigation of the convective heat transfer and friction factor of magnetic Ni nanofluids within cylindrical pipes, International Journal of Thermofluid Science and Technology 8(1) (2021) 080101.

[6] R.M. Terrill, Laminar flow in uniformly porous channel, Aeronautical Quarterly 15(3) (1964) 299-310.

[7] C. Zhou, J. Majdalani, Improved mean-flow solution for slab rocket motors with regressing walls, Journal of Propulsion and Power 18(3) (2002) 703-711.

[8] R. Akhter, M.M. Ali, MHD natural convection in nanofluid filled square cavity with isothermally heated hexagonal block, International Journal of Thermofluid Science and Technology 9 (1) (2022) 090104.

[9] Y. Belkassmi, L. Elmaimouni, A. Rafiki, K. Gueraoui, N. Hassanain, Heat and mass transfer modeling during laminar condensation of non-cryogenic downward fluids flow in a small vertical tube, International Journal of Thermofluid Science and Technology 7(4) (2020) 070401.

[10] S. Hamrelaine, F. Mebarek-Oudina, M.R. Sari, Analysis of MHD Jeffrey Hamel flow with suction/injection by homotopy analysis method, Journal of Advanced Research in Fluid Mechanics and Thermal Sciences 58(2) (2020) 173-186.

[11] M. Gudekote, R. Choudhari, Slip effects on peristalic transport of casson fluid in an inclined elastic tube with porous walls, Journal of Advanced Research in Fluid

Mechanics and Thermal Sciences 43(1) (2020) 67-80.

[12] S.M. Cox, Two-dimensional flow of a viscous fluid in a channel with porous walls, Journal of Fluid Mechanics 227 (1991) 1-33.

[13] P. Watson, W.H.H. Banks, M.B. Zaturska, P.G. Drazin, Laminar channel flow driven by accelerating walls, European Journal of Applied Mathematics 2(4) (1991) 359- 385.

[14] E.B.B. Watson, W.H.H. Banks, M.B. Zaturska, P.G. Drazin, On transition to chaos in two-dimensional channel flow symmetrically driven by accelerating walls, Journal of Fluid Mechanics 212 (1990) 451- 485.

[15] J.F. Brady, A. Acrivos, Steady flow in a channel or tube with an accelerating surface velocity: An exact solution to the Navier-Stokes equations with reverse flow, Journal of Fluid Mechanics 112 (1981) 127-150.

[16] E. Magyari, B. Keller, Exact solutions for self-similar boundary-layer flows induced by permeable stretching walls, European Journal of Mechanics B-Fluids 19(1) (2000) 109-122.

[17] J. Hona, M.M. Nganbe II, Modelling and simulation of an industrial flow between two moving permeable surfaces, International Journal of Engineering Systems Modelling and Simulation, Vol. 9 (4) (2017) 177-187.

[18] S. Dinarvand, M.M. Rashidi, A reliable treatment of a homotopy analysis method for two- dimensional viscous flow in a rectangular domain bounded by two moving porous walls, Nonlinear Analysis: Real World Applications 11(3) (2010) 1502-1512.

[19] J. Majdalani, C. Zhou, Moderate-to-large injection and suction driven channel flows with expanding and contracting walls, ZAMM 83 (3) (2003) 181-196.

[20] A.S. Berman, Laminar flow in channels with porous walls, Journal of Applied Physics 24(9) (1953) 1232-1235.

[21] M.M. Nganbe II, E. Ngo Nyobe, J. Hona, E. Pemha, Heat transfer and circular flow around a hydrodynamic turning point through a porous annular tube, Chinese Journal of Physics 61 (2019) 316-335.

[22] W.H.H. Banks, M.B. Zaturska, On flow through a porous annular pipe, Physics of Fluids A 4(6) (1992) 1131-1141.

[23] M.B. Zaturska, W.H.H. Banks, Suction-driven flow in a porous pipe, Journal of Applied Mathematics and Mechanics (ZAMM) 75(1) (1995) 21-30.

[24] J. Majdalani, G.A. Flandro, The oscillatory pipe flow with arbitrary wall injection, Proceedings of the Royal Society of London A 458(2023) (2002) 1621-1651.

[25] J. Hona, E. Ngo Nyobe, E. Pemha, Dynamic behavior of a steady flow in an annular tube with porous walls at different temperatures, International Journal of Bifurcation and Chaos in Applied Sciences and Engineering 19(9) (2009) 2939-2951.

[26] J. Hona, E. Ngo Nyobe, E. Pemha, Creeping flow with non-uniform viscosity in a permeable industrial conduct, International Journal of Engineering Systems Modelling and Simulation 8(3) (2016) 183-194.

[27] A.D. MacGillivray, C. Lu, Asymptotic solution of a laminar flow in a porous channel with large suction: A nonlinear turning point problem, Methods and Applications of Analysis 1(2) (1994) 229-248.

[28] S.K. Karode, Laminar flow in channels with porous walls, revisited, Journal of Membrane Science, Vol. 191(1-2) (2001) 237-241.

[29] Z. Abbas, J. Hasnain, S. Aly, M. Sheikh, Comparative analysis for partial slip flow of ferrofluid Fe3O4 nanoparticles in a semi-porous channel, Journal of King Saud University Science 32(5) (2020) 2646-2655.

[30] Z. Bano, A. Siddiqui, K. Bhatti, Unsteady Stokes flow through a porous pipe with periodic suction and injection with slip conditions, Journal of Applied and Computational Mechanics 6 (2020) 1168-1177.

[31] S. Ferro, G. Gnavi, Spatial stability of similarity solutions for viscous flows in channels with porous walls, Physics of Fluids 12(4) (2000) 797-802.

[32] S. Ferro, G. Gnavi, Effect of temperature-dependent viscosity in channels with porous walls, Physics of Fluids 14(4) (2002) 839-849.

[33] Y. Sun, P. Lin, L. Li, Temporal stability analysis for multiple similarity solutions of viscous incompressible flows in porous channels with moving walls, Applied Mathematical Modeling 77 (2020) 738-755.

[34] J. Griffond, G. Casalis, On the dependence on the formulation of some nonparallel stability approaches applied to the Taylor flow, Physics of Fluids 12(2) (2000) 466-468.

[35] J. Griffond, G. Casalis, On the nonparallel stability of the injection induced two-dimensional Taylor flow, Physics of Fluids 13(6) (2001) 1635-1644.

[36] J. Barron, W.K. Van Moorhem, J. Majdalani, A novel investigation of the oscillatory field over a transpiring surface, Journal of Sound and Vibration 235(2) (2000) 281-297..

[37] N. Bildik, A. Konuralp, The use of variational iteration method, differential transform method and Adomian decomposition method for solving different types of nonlinear partial

differential equations, International Journal of Nonlinear Sciences and Numerical Simulation 7(1) (2006) 65-70.
[38] M. Shahzad, M. Ali, F. Sultan, W. A. Khan, Z. Hussain, Theoretical analysis of cross-nanofluid flow with nonlinear radiation and magnetohydrodynamics, Indian Journal of Physics 95(3) (2021) 481-488.
[39] G.D. Smith, Numerical solution of partial differential equations: finite difference methods (3rd ED.), Oxford University Press, 1985.
[40] M.H. Carpenter, D.I. Gottlieb, S.S. Abarbanel, Time-stable boundary conditions for finite-difference schemes solving hyperbolic systems: methodology and application to high-order compact schemes, Journal of Computational Physics 111(2) (1994) 220-236.
[41] R.B. Bird, W.E. Stewart, E.N. Lightfoot, Transport phenomena, 2nd edition, Wiley: NY, 2002.
[42] R.B. Bird, R.C. Armstrong, O. Hassager, Dynamics of polymeric fluids: Volume 1 Fluid Mechanics, Wiley: NY, 1987.
[43] W.M. Kays, Convective heat and mass transfer, McGraw-Hill, New York, 1966.
[44] M.F. White, Viscous fluid flow, McGraw-Hill, New York, 1991.
[45] F.R.P. Lehel, J. Hona, Similarity solutions of the Navier-Stokes equations for an injection-driven flow between two orthogonally moving porous discs, Chinese Journal of Physics 73 (2021) 360-374.
[46] M. Goto, S. Uchida, Unsteady flows in a semi-infinite expanding pipe with injection through wall, Transactions of the Japanese Society for Aeronautical and Space Sciences 38(434) (1990) 131-138.
[47] G.P. Sutton, Rocket Propulsion Elements, 6th ed., Wiley, New York, 1992.
[48] R.C. Reid, J.M. Prausnitz, B. E. Poling, The Properties of gases and liquids, 4th ed., McGraw-Hill, New York, 1987.
[49] E.C. Dauenhauer, J. Majdalani, Exact self-similarity solution of the Navier–Stokes equations for a porous channel with orthogonally moving walls, Physics of Fluids 15(6) (2003)1485-1495.
[50] T. Fang, J. Zhang, Flow between two stretchable disks-An exact solution of the Navier–Stokes equations, International Communications in Heat and Mass Transfer 35(8) (2008) 892-895.
[51] J.R. Sellars, Laminar flow in channels with porous walls at high suction Reynolds numbers, Journal of Applied Physics 26(4) (1955) 489-490.